Maintenance of spatial gene expression by Polycomb-mediated repression after formation of a vertebrate body plan

Running title: PcG repression in zebrafish

Authors: Julien Rougeot[1,2*], Naomi D. Chrispijn[1], Marco Aben[1,2], Dei M. Elurbe[1,2], Karolina M. Andralojc[1], Patrick J. Murphy[3,4], Pascal W.T.C. Jansen[5], Michiel Vermeulen[5], Bradley R. Cairns[3], Leonie M. Kamminga[1,2,*]

Affiliations: [1]Radboud University, Faculty of Science, Department of Molecular Biology, Radboud Institute for Molecular Life Sciences, Nijmegen, the Netherlands [2]Radboud University Medical Center, Department of Molecular Biology, Nijmegen, the Netherlands [3]Howard Hughes Medical Institute, Department of Oncological Sciences and Huntsman Cancer Institute, University of Utah School of Medicine, Salt Lake City, UT 84112, USA [4]Wilmot Cancer Institute, Rochester Center for Biomedical Informatics, University of Rochester Medical Center, Rochester, NY [5]Radboud University, Department of Molecular Biology, Faculty of Science, Radboud Institute for Molecular Life Sciences, Oncode Institute, Nijmegen, The Netherlands. *Corresponding authors.

Corresponding author's email address: l.kamminga@science.ru.nl ; julien.rougeot@wur.nl

Key words: Polycomb, Ezh2, zebrafish, ChIP-seq, RNA-seq, proteomics

Summary statement

Our unique zebrafish model of maternal and zygotic mutant for the *Polycomb* group gene *ezh2* reveals major conserved and divergent mechanisms in epigenetic gene repression during vertebrate development.

Abstract

Polycomb group (PcG) proteins are transcriptional repressors that are important regulators of cell fate during embryonic development. Among them, Ezh2 is responsible for catalyzing the epigenetic repressive mark H3K27me3 and is essential for animal development. The ability of zebrafish embryos lacking both maternal and zygotic *ezh2* to form a normal body plan provides a unique model to comprehensively study Ezh2 function during early development in vertebrates. By using a multi-omics approach, we found that Ezh2 is required for the deposition of H3K27me3 and is essential for the recruitment of Polycomb group protein Rnf2. However, and despite the complete absence of PcG-associated epigenetic mark and proteins, only minor changes in H3K4me3 deposition and gene and protein expression occurred. These changes were mainly due to local deregulation of transcription factors outside their normal expression boundaries. Altogether, our results in zebrafish show that Polycomb-mediated gene repression is important right after the body plan is formed to maintain spatially restricted expression profiles of transcription factors and highlight the differences that exist in the timing of PcG protein action between vertebrate species.

42 **Introduction**

43 Development of multi-cellular organisms involves highly dynamic and controlled processes during
44 which one single totipotent cell will multiply and differentiate into all the cells composing the adult
45 individual. Specification of cell identity is controlled through the establishment of spatially and
46 temporally restricted transcriptional profiles, which are subsequently maintained by epigenetic
47 mechanisms (Brock and Fisher, 2005). Epigenetic maintenance of gene expression can act through
48 modifications of the chromatin, the complex of DNA wrapped around an octamer of histones H2A,
49 H2B, H3, and H4 and its associated proteins and non-coding RNAs, creating an epigenetic landscape,
50 often referred to as the epigenome (Zhu and Li, 2016). These modifications can be propagated from
51 mother to daughter cells and thereby maintain gene expression profiles by controlling the
52 accessibility of the DNA to the transcriptional machinery (Li and Reinberg, 2011).

53 Important regulators of the epigenome during development are the Polycomb Group (PcG) proteins.
54 First identified in *Drosophila melanogaster*, PcG proteins were found to maintain the pre-established
55 pattern of *hox* gene expression (Kennison, 1995). Subsequent studies showed that PcG proteins are
56 important for proper patterning during early embryonic development, tissue-specific development,
57 and maintenance of the balance between pluripotency and differentiation of stem cells in multiple
58 species (Schuettengruber et al., 2017). Two main PcG complexes have been described (Chittock et
59 al., 2017). The Polycomb Repressive Complex 2 (PRC2) is composed of the core subunits EZH1/2
60 (Enhancer of Zeste Homologue 1/2), SUZ12 (Supressor of Zeste 12), and EED (Embryonic Ectoderm
61 Development). EZH2 has a catalytically active SET domain that trimethylates lysine 27 of histone H3
62 (H3K27me3), an epigenetic mark associated with gene repression and found along gene coding
63 sequences (Mikkelsen et al., 2007). The catalytic subunits of PRC2 are mutually exclusive and EZH1 is
64 postulated to complement the function of EZH2 in non-proliferative adult organs (Margueron et al.,
65 2008, Shen et al., 2008). H3K27me3 can be recognized by the Polycomb Repressive Complex 1
66 (PRC1). A diversity of PRC1 compositions has been described and canonical PRC1 is composed of the
67 core subunits RING1/RNF2 (Ring Finger Protein 2 a/b), PCGF1-6 (Polycomb Group RING fingers 1-6),
68 PHC (Polyhomeotic), and CBX (Chromobox homolog) (Gao et al., 2012, Kloet et al., 2016). PRC1
69 catalyzes the ubiquitination of lysine 119 of histone H2A (H2AK1119ub) and strengthens gene
70 repression. In contrast to this canonical view, recent studies implicate that PRC1 is also active in the
71 absence of PRC2 (He et al., 2013, Loubiere et al., 2016, Tavares et al., 2012). Trithorax Group (TrxG)
72 proteins antagonize PcG protein function through the deposition of a trimethyl group on lysine 4 of
73 histone H3 (H3K4me3) on promoters and enhancers from virtually all transcribed genes (Klymenko
74 and Muller, 2004, Schmitges et al., 2011, Santos-Rosa et al., 2002).

In mice, loss of PRC2 genes *Ezh2*, *EED*, or *Suz12* or PRC1 gene *Rnf2* leads to post-implantation embryonic lethality during early gastrulation (O'Carroll et al., 2001, Faust et al., 1998, Pasini et al., 2004, Voncken et al., 2003), making it difficult to study transcriptional regulation by PcG complexes during early development. Apart from the mouse model, very few studies have focused on functional characterization of PcG function during vertebrate development, and especially studies involving genetic mutants for different PcG genes. Lately, the zebrafish embryo has emerged as a model of choice to study developmental epigenetics in vertebrates (Chrispijn et al., 2019, Lindeman et al., 2011, Murphy et al., 2018, Potok et al., 2013, Vastenhouw et al., 2010). Others and we previously used loss-of-function mutants to show that *ezh2* is essential for zebrafish development (Dupret et al., 2017, San et al., 2016, San et al., 2018, Zhong et al., 2018). More particularly, our unique vertebrate model of zebrafish embryos mutant for both maternal and zygotic *ezh2*, referred as *MZezh2* mutant embryos, develop seemingly normal until 1 dpf, forming a proper body plan. These mutants ultimately die at 2 dpf, exhibiting a 100% penetrant pleiotropic phenotype associated with a loss of tissue maintenance (San et al., 2016). This makes zebrafish *MZezh2* mutant embryos a unique model to study the function of Ezh2 during early development, from fertilization to tissue specification, in the unique context of a vertebrate embryo in which trimethylation of H3K27 has never occurred, unlike cell culture, conditional, or zygotic mutant models.

We conducted a multi-omics approach in these *MZezh2* mutant embryos to study how PcG-mediated gene regulation controls axis formation and tissue specification. We focused our study on 24 hours post fertilization (hpf) embryos, when the first phenotypes become visible, and the anterior-posterior patterning of the embryos is properly established. Our results show conservation of basic PcG recruitment and silencing mechanisms and reveal that proper PRC2 function is essential for Rnf2 recruitment. However, very surprisingly, and despite the complete absence of PcG proteins and their associated epigenetic marks on the chromatin, the transcriptional and proteomic profile of *MZezh2* mutant embryos remains largely unchanged compared to wildtype embryos. The changes affect primarily a subset of PcG target genes. These genes are mainly transcription factors essential for developmental processes which present locally restricted aberrant gene expression. Our results show that zebrafish embryo development is initially independent of PcG repression until the stage of tissue maintenance and stress the differences that exist in the timing of PcG function requirement between vertebrate species.

107 **Results**

108 **The repressive epigenetic mark H3K27me3 is absent in *MZezh2* embryos**

109 To study the function of Ezh2 during development, we used the *ezh2* nonsense mutant allele *ezh2*
110 *(hu5670)* containing a premature stop codon within the catalytic SET domain, resulting in the
111 absence of Ezh2 protein (San et al., 2016). Total elimination of both maternal and zygotic
112 contribution of Ezh2 protein and RNA, by using the germ cell transplantation technique described
113 previously (Ciruna et al., 2002, San et al., 2016), allowed us to study the function of Ezh2 during early
114 development. As previously shown, *MZezh2* mutant embryos display normal body plan formation
115 and a mild phenotype at 24 hpf. They die at 48 hpf, at which point pleiotropic phenotypes are
116 observed, such as smaller eyes, smaller brain, blood coagulation, and absence of pectoral fins
117 (Figure. 1A). Western Blot analysis at 3.3 hpf and 24 hpf confirmed the absence of both maternal
118 and zygotic Ezh2 in these mutants, respectively (Figure 1B). In addition, our previous study also
119 reported that H3K27me3 was not detectable in *MZezh2* mutants by immunofluorescence (San et al.,
120 2016).

121 To further confirm the absence of Ezh2 in *MZezh2* mutants and its effect on H3K27me3 deposition,
122 we performed ChIP-sequencing (ChIP-seq) for Ezh2 and H3K27me3 at 24 hpf in both wildtype and
123 *MZezh2* mutant embryos. ChIP-seq analyses for Ezh2 and H3K27me3 revealed 816 and 3,353 peaks
124 in wildtype embryos, respectively (Figure 1C, Table S1). Although the number of peaks differed
125 between the two proteins, their binding profiles greatly overlap (Figure 1E). Quantification showed
126 that 85% of Ezh2 peaks also contain H3K27me3 (Fig. S1A). Known PcG target genes such as the
127 *hoxab* gene cluster, *tbx* genes, and *gsc* presented similar binding profiles for Ezh2 as for H3K27me3
128 (Figure 1F,G, Fig. S1B), whereas the ubiquitously expressed genes *eif1ad* and *tbp* showed absence of
129 both Ezh2 and H3K27me3 (Fig. S1B).

130 In *MZezh2* mutant embryos, the binding of Ezh2 and H3K27me3, as detected by ChIP-seq, was
131 virtually absent, with 3 and 22 peaks detected for Ezh2 and H3K27me3, respectively (Figure 1C).
132 Manual inspection of these remaining peaks revealed that they are present in gene deserts and low
133 complexity regions and are most probably artefacts (Fig. S1B). Ezh2 and H3K27me3 coverage was
134 reduced to background levels in *MZezh2* mutants compared to wildtype (Figure 1D). Finally, the
135 *hoxab* gene cluster*, tbx3a, tbx5a*, *gsc,* and *isl1* loci, targeted by PcG repression in wildtypes, also
136 showed a complete absence of Ezh2 and H3K27me3 binding in *MZezh2* mutants (Figure 1F,G, Fig.
137 S1B).

138 In order to rule out the possibility that the absence of detection of Ezh2 and H3k27me3 in *MZezh2*
139 mutant samples was due to an inefficient ChIP-seq or a normalization artifact specific to mutant
140 samples, the second ChIP-seq replicates for both Ezh2 and H3K27me3 were conducted with spike-in
141 chromatin control. After normalization using the immunoprecipitated spike-in chromatin, the
142 decrease in Ezh2 and H3K27me3 coverage in mutant compared to wildtype appear even higher than
143 without normalization, both at genome-wide level (Fig. S2A,B) and on target genes (Fig. S2C).

144 Altogether, these results demonstrate that *MZezh2* mutants exhibit complete absence of Ezh2 and
145 H3K27me3 from chromatin.

146

147 **Loss of PRC2-mediated repression results in loss of PRC1 recruitment during early development**

148 It is postulated that PRC1 is recruited to chromatin by PRC2-deposited H3K27me3 but can also have
149 a function independent of PRC2 (He et al., 2013, Loubiere et al., 2016, Tavares et al., 2012). As both
150 Ezh2 and H3K27me3 are absent from *MZezh2* mutant embryos, we investigated whether PRC1 is still
151 recruited to chromatin in these mutants. In zebrafish, Rnf2 is the only catalytic subunit of PRC1 (Le
152 Faou et al., 2011). ChIP-seq for Rnf2 in wildtype embryos at 24 hpf reveals 837 peaks (Figure 1C,
153 Table S1) which are present at Ezh2 and H3K27me3 positive regions (Figure 1E). We found that 70%
154 of Ezh2 peaks were also positive for Rnf2 in wildtype embryos (Fig. S1A).

155 In *MZezh2* mutant embryos, only 14 binding sites could be detected for Rnf2 (Figure 1C) and Rnf2
156 average binding (measured in RPKM) was reduced to background level, as observed for Ezh2 and
157 H3K27me3 binding (Figure 1C,E). This loss of Rnf2 was observed at both gene clusters such as *hoxab*
158 (Figure 1F) and individual transcription factors such as *tbx3a*, *tbx5a*, and *gsc* (Figure 1G, Fig. S1B). As
159 for Ezh2 and H3K27me3, Rnf2 remaining peaks in *MZezh2* mutant embryos were detected in
160 intergenic regions with repeat sequences and are most probably artefacts (Fig. S1D).

161 Furthermore, H2AK119ub was not detectable in core histone extracts from *MZezh2* mutant embryos
162 (Fig. S1B), suggesting a total absence of functional recruitment of canonical PRC1 in absence of Ezh2.

163

164 **Loss of H3K27me3 in *MZezh2* mutant embryos induces gene specific gain of H3K4me3**

165 As PcG and TrxG complexes are known to have an antagonistic effect on gene expression (Piunti and
166 Shilatifard, 2016), we investigated whether the loss of H3K27me3 in *MZezh2* mutant embryos
167 changed the deposition H3K4me3, a mark associated with gene activation.

168 To this aim, we performed ChIP-seq for H3K4me3 in triplicates in both wildtype and *MZezh2* mutant
169 embryos at 24 hpf. We observed a similar distribution of H3K4me3 peaks, with 10,556 peaks
170 detected in wildtype embryos and 10,096 in *MZezh2* mutants (Figure 2A, Table S1). A majority of
171 9550 peaks were shared between wildtype and *MZezh2* mutant embryos (Figure 2A), suggesting
172 little to no differences in H3K4me3 deposition in absence of Ezh2.

173 We next assessed the differences in H3K4me3 peak intensity upon loss of Ezh2 by performing
174 differential binding analysis using DiffBind. We identified 95 peaks with an enriched H3K4me3
175 deposition and 28 peaks with a decrease H3K4me3 intensity (Fig 2B). Comparison with Ezh2 and
176 H3K27me3 ChIP-seq show an over-representation of PcG targets among the peaks enriched in
177 H3K4me3 upon loss of Ezh2 (Fig 2C). A majority of the peaks enriched for H3K4me3 are PcG targets,
178 with 71% (68 out of 95) targeted by Ezh2 and 75% (71 out of 95) by H3K27me3, which is more than
179 expected by chance. On the opposite, peaks with a decrease of H3K4me3 deposition show little to
180 no enrichment in PcG targets (Fig 2D). This result shows that the targets of PcG repression in
181 wildtype are more susceptible to gain H3K4me3 upon loss of Ezh2/H3K27me3.

182 We then searched for the closest genes from the regions with increased H3K4me3 peak coverage
183 detected by DiffBind and identified 118 genes. For example, the transcription factors *hoxa13b*,
184 *tbx5a*, and *gsc* showed enrichment for H3K4me3 close to their promoter (Fig 2E). Gene ontology
185 analysis revealed that these genes were mainly involved in transcriptional regulation and organismal
186 development (Figure 2F). Among these 118 identified genes, 51 encode for transcription factors,
187 among which were members of the *hox*, *tbx*, *sox*, and *pax* gene families, known targets of PcG
188 complexes.

189 These results show that loss of PcG repression has a limited effect on H3K4me3 active epigenetic
190 mark at 24 hpf, and that the genes presenting an increase in H3K4me3 deposition are mainly
191 transcription factors directly targeted by PcG repression.

192

193 **Epigenetic changes in *MZezh2* mutant embryos induce upregulation of transcription factors**

194 As *MZezh2* mutant embryos show a complete lack of the H3K27me3 repressive mark and a subtle
195 yet selective increased deposition of H3K4me3 activating mark on genes coding for transcription
196 factors, we investigated the effect of loss of Ezh2 on the transcriptome and proteome of wildtype
197 and *MZezh2* mutant embryos at 24 hpf.

198 Transcriptome analysis by RNA-seq in the two conditions revealed a limited effect on the
199 transcriptome upon the loss of Ezh2. Only 60 genes were detected to be significantly upregulated
200 ($log_2FC \geq 1$ and *P*-adj < 0.05) and 28 genes downregulated ($log_2FC \leq -1$ and *P*-adj < 0.05) in *MZezh2*
201 mutants (Figure 3A). The proteome analysis, identified 111 upregulated ($log_2FC \geq 1.5$ and *P-adj* <
202 0.05) and 110 downregulated ($log_2FC \leq -1.5$ and *P-adj* < 0.05) proteins in *MZezh2* mutants compared
203 to wildtype controls.

204 GO analysis showed that the deregulated genes in the transcriptomics data are associated to control
205 of organism development and regulation of transcription (Fig 3C). The proteins deregulated in the
206 proteome analysis also revealed anatomy terms associated to organs presenting clear phenotypes in
207 the *MZezh2* mutant embryos (Fig 3D).

208 When comparing our RNA-seq results with our ChIP-seq data, we found that 60% (36 out of 60) of
209 the upregulated genes are targets of H3K27me3, which is more than expected by chance.
210 Furthermore, a significant proportion (27%) of these genes also shows an increase in H3K4me3
211 deposition upon loss of Ezh2 whereas none show a decrease in H3K4me3 (Fig 3E). The
212 downregulated genes also show some significant association with H3K27me3 but did not show any
213 correlation with gain or loss of H3K4me3 deposition (Fig 3E). However, the proteomics data did not
214 present any correlation with either the ChIP-seq or the RNA-seq results (Fig 3F).

215 Finally, proteome data indicate that, in addition to Ezh2, Suz12b is downregulated in *MZezh2* mutant
216 embryos (Figure 4A). Other PRC2 subunits were either not detected or not significantly
217 downregulated. Subunits of the canonical PRC1 complex were mostly not detected or not
218 significantly overexpressed (Fig. S3).

219

220

221 **Loss of *ezh2* results in expression of *hox* genes outside their normal expression domains**

222 We next carried out a spatial expression analysis on selected target genes to distinguish between the
223 possibilities that absence of PcG-mediated repression leads to global but moderate gene
224 deregulation or to deregulation limited to specific cell types or tissues.

225 To start with, we focused on expression of different genes from the *hox* gene family. These genes
226 are known targets of Polycomb-mediated repression (Mallo and Alonso, 2013) and some of them
227 have been previously shown to be deregulated in *MZezh2* mutant embryos (San et al., 2016). Every

228 *hox* gene has an expression pattern that is restricted along the anterior-posterior axis (Prince et al.,
229 1998). To obtain spatially resolved data along the anterior-posterior axis, we performed RT-qPCR on
230 the anterior half and the posterior half of 24 hpf wildtype and *MZezh2* mutant embryos. We then
231 compared the normalized relative expression levels between the different halves of the *MZezh2*
232 mutant and wildtype embryos. The tested *hox* genes were selected based on their domain of
233 expression along the anterior-posterior axis (Figure 5A-D). The *hoxa9a* gene, whose expression
234 extends to anterior, until slightly outside the posterior half of the embryos, showed, as expected, a
235 higher expression in the posterior part than in the anterior part in wildtype embryos (Figure 5A). In
236 *MZezh2* mutants, *hoxa9a* was overexpressed in the anterior compartment compared with wildtype
237 embryos, reaching levels similar to those observed in the posterior part of wildtype embryos. No
238 significant differences were detected in the level of expression when comparing the posterior
239 compartment of *MZezh2* mutant and wildtype embryos (Figure 5A). Similar results were obtained for
240 *hoxa9b*, where overexpression was detected in the anterior compartment of *MZezh2* mutant
241 embryos compared to the anterior compartment of wildtype embryos (Figure 5B). The *hoxa11b* and
242 *hoxa13b* genes, which are expressed primarily posterior, showed, as expected, higher expression in
243 the posterior half of the wildtype embryos compared to the anterior half (Figure 5C,D). In the
244 *MZezh2* mutant embryos, both *hox* genes were upregulated in the anterior half of the *MZezh2*
245 mutant embryos compared to wildtypes (Figure 5C,D) but their expression level remained lower
246 than in the posterior half of the wildtype embryos (Figure 5C,D).

247 These comparative analyses of anterior and posterior parts of the embryo suggest that, upon loss of
248 Ezh2, *hox* genes show an ectopic anterior expression while keeping wildtype expression levels in
249 their normal expression domains.

250

251 **Different transcription factors show various profiles of deregulation in the absence of Ezh2**

252 To further pursue our investigation on the changes in gene expression patterns in absence of Ezh2,
253 we performed *in situ* hybridization (ISH) on members from the *tbx* gene family of transcription
254 factors. The *tbx2a*, *tbx2b*, *tbx3a*, and *tbx5a* genes have partial overlapping expression patterns in
255 wildtype embryos, but also display gene specific expression domains (Figure 6A). At 24 hpf, these *tbx*
256 gene family members are expressed in the dorsal region of the retina, in the heart, and the pectoral
257 fins (Ribeiro et al., 2007, Tamura et al., 1999). In addition, the genes *tbx2a*, *tbx2b*, and *tbx3a* are
258 expressed in the otic vesicle. The genes *tbx2b* and *tbx3a* are expressed in different ganglions and
259 neurons in anterior and posterior regions of wildtype embryos (Ribeiro et al., 2007). Finally,

260 expression of *tbx2b* can also be detected in part of pharyngeal arches 3-7 and the distal region of the
261 pronephros and *tbx3a* expression can be detected in the brachial arches (Thisse, 2004). This spatial
262 prevalence of *tbx* gene expression in the anterior half of the embryo was also detected by RT-qPCR
263 at 24 hpf, where *tbx2a*, *tbx2b* and *tbx5a* expression was significantly higher in the anterior than in
264 the posterior part of wildtype embryos (Figure 6B).

265 ISH for these *tbx genes* on *MZezh2* mutant embryos at 24 hpf suggests ectopic expression of these
266 transcription factors around their normal expression pattern in the eye, the otic vesicle, and the
267 heart, except for *tbx2b* (Figure 6A). This scattering in gene expression was reflected in a trend
268 towards a higher expression in the anterior half of *MZezh2* mutant embryos as detected by RT-qPCR,
269 although only *tbx2a* and *tbx5a* results were significant (Figure 6B). In addition, ISH for *tbx5a*, and to
270 a lesser extent *tbx3a*, showed ubiquitous expression throughout the entire body of *MZezh2* mutants
271 which was not visible in wildtypes (Figure 6A). RT-qPCR results confirmed increased expression of
272 *tbx5a* in both the anterior and posterior half of the *MZezh2* mutant embryos (Figure 6B).

273 Beside the observed ectopic expression, all tested *tbx* genes showed absence of expression in
274 specific structures upon Ezh2 loss. For example, in *MZezh2* mutant embryos, all four *tbx* genes
275 showed no expression in the fin bud (Figure 6A). In *MZezh2* mutant embryos, the gene *tbx2b*
276 showed no expression in the pharyngeal arches 3-7 and the lateral line ganglions, and *tbx3a* was not
277 observed in the branchial arches (Fig 6a). This absence of expression was not detected by RT-qPCR
278 (Figure 6B) but a trend toward downregulation for *tbx2b* was observed in RNA-seq results on whole
279 *MZezh2* mutant embryo lysates (Figure 6C).

280 In addition, we tested transcription factors from other families which were targeted by H3K27me3 in
281 wildtype. The transcription factor *isl1*, expressed in all primary neurons (Dyer et al., 2014), showed a
282 similar absence of expression in the fin bud and the cranial motor neurons in the midbrain
283 (trigeminal, facial and vagal motor neurons), as observed for *tbx2a*. Its expression was also absent in
284 the ventral region of the eye, the facial ganglia, and in the pronephros from *MZezh2* mutant
285 embryos, where it is normally expressed in wildtype embryos (Heisenberg et al., 1999, Zhang et al.,
286 2017) (Figure 6A). This loss in expression in *MZezh2* mutant embryos was not detected by RT-qPCR
287 but a clear tendency toward downregulation was detected by RNA-seq (Figure 6B,C). Even more
288 surprising was the expression pattern of *gsc* in the *MZezh2* mutant embryos. Whereas all the
289 wildtype embryos show highly specific expression in the telencephalon and diencephalon nuclei, the
290 branchial arches, and the otic vesicle (Thisse, 2004), *gsc* expression was lost and instead ubiquitous
291 expression was observed in *MZezh2* mutant embryos (Figure 6A). This observation was confirmed by

292 RT-qPCR and RNA-seq where upregulation of *gsc* was clearly detected in *MZezh2* mutant embryos
293 (Figure 6B,C).

294 Taken together, these spatial expression analyses showed that the tested transcription factors are
295 expressed outside their normal wildtype expression boundaries in *MZezh2* mutant embryos at 24
296 hpf. Furthermore, expression of some of these genes is lost in specific tissues in the *MZezh2* mutant
297 embryos.

298

299

300 **Discussion**

301 Here, we showed for the first time the genome-wide binding patterns of Ezh2 and Rnf2, the catalytic
302 subunits of PRC2 and PRC1, respectively, in 24 hpf zebrafish embryos. The overall overlap between
303 the binding patterns of Ezh2, Rnf2, and the PcG related epigenetic mark H3K27me3 suggests that the
304 PcG-mediated gene repression mechanisms (Chittock et al., 2017) are evolutionary conserved in
305 zebrafish development. The complete loss of H3K27me3 in *MZezh2* mutant embryos reveals that
306 Ezh2 is the only methyltransferase involved in trimethylation of H3K27 during early zebrafish
307 development. This result was expected as Ezh1, the only other H3K27me3 methyltransferase, was
308 shown by a number of studies not to be maternally loaded nor expressed in the zebrafish embryo
309 until at least after 1 dpf (Chrispijn et al., 2018, San et al., 2016, Sun et al., 2008, White et al., 2017).
310 In addition, proteomics results showed decreased protein expression of most PRC2 subunits. This
311 could indicate a destabilization of PRC2 in absence of the catalytic subunit in *MZezh2* mutant
312 embryos. We could therefore confirm that zebrafish embryos can form a normal body plan in
313 absence of PRC2-mediated gene repression.

314 The total loss of Rnf2 binding in the *MZezh2* mutants suggests that only the canonical pathway, in
315 which PRC2 is required for PRC1 recruitment, is active during this stage of development. This
316 absence of PRC1 recruitment to the chromatin is not caused by an absence of the complex in the
317 *MZezh2* mutants, since most of the PRC1 subunits were detectable and not deregulated as shown by
318 proteomic analysis. This is in contrast with studies in cultured mouse embryonic stem cells where
319 non-canonical PRC1 complexes were shown to be recruited to developmental regulated genes
320 independently of PRC2 (He et al., 2013, Tavares et al., 2012). This difference could be explained by
321 the complete absence of H3K27me3 as from fertilization onwards in *MZezh2* mutant embryos,
322 whereas other studies used conditional knockdown. Therefore, our model suggests that the PRC2-

323 independent recruitment of PRC1 during early development can occur if PRC1 recruitment was first
324 primed by a PRC2-dependent mechanism happening earlier during development.

325 As repressive and activating marks are known to antagonize each other (Schmitges et al., 2011), one
326 could expect an increase in the H3K4me3 level deposited by TrxG proteins in absence of H3K27me3
327 associated with an increase in gene activation. However, the effects on H3K4me3 deposition, gene
328 expression, and protein expression are limited in *MZezh2* mutant embryos at 24 hpf. This
329 observation is in agreement with the near complete absence of phenotype at this developmental
330 time point. Thus, it appears that transcriptional regulation during zebrafish development is largely
331 PRC2-independent until later stages of development, when maintenance of cellular identity is
332 required. These results were unexpected, as PRC2 is described to be essential during mammalian
333 development already during gastrulation (Faust et al., 1998, O'Carroll et al., 2001, Pasini et al., 2004).
334 It implies, that even if PcG-mediated repression mechanisms are conserved, the developmental
335 stages at which these mechanisms are required differ between species. Possibly, the external
336 development of the zebrafish and its rapid early development could explain this difference in
337 phenotype.

338 Although limited, genes that show a gain in H3K4me3 deposition or in expression upon loss of *ehz2*
339 are mainly transcription factors targeted by H3K27me3 in wildtype embryos. That only a minor
340 fraction of all H3K27me3 target genes gained expression (36 out of 2610 = 1.2%, Fig 3E) suggests
341 different mechanisms of regulation of PcG target genes at this time. Our hypothesis is that control of
342 gene expression by signaling pathways and transcription factor networks (McGinnis and Tickle, 2005)
343 is a robust mechanism and can be maintained until 1 dpf in absence of repression by PcG complexes.
344 At 1 dpf, in absence of PcG-mediated repression, the first derepressed genes will be the genes
345 subjected to the most fine-tuned transcriptional control, such as genes controlled by precise
346 morphogen gradients. For example, it was shown that PRC2 attenuates expression of genes
347 controlled by retinoic acid signaling (Laursen et al., 2013, Zhang et al., 2014). In vertebrates, and
348 most particularly zebrafish, retinoic acid signaling is responsible for induction of formation of, among
349 others, the forelimb field (Cunningham et al., 2013, Grandel and Brand, 2011), dorsoventral
350 patterning of eyes (Lupo et al., 2005, Marsh-Armstrong et al., 1994), hindbrain patterning (Maves
351 and Kimmel, 2005), *hox* gene expression (White et al., 2007), and the development of other organs
352 (Samarut et al., 2015). All these processes are affected in *MZezh2* mutant embryos at 24 hpf and
353 onwards and, therefore, could be explained by a defect in the response to retinoic acid signaling.

354 Spatial analysis of gene expression revealed different effects on gene expression patterns caused by
355 loss of Ezh2. Anterior-posterior specific RT-qPCR showed that *hox* genes become abnormally

356 expressed in the anterior half of the *MZezh2* mutant embryos; whereas expression levels in the
357 posterior half remained unchanged. These results are in agreement with previous studies showing
358 ectopic expression of *hox* genes in PRC1 and PRC2 zebrafish mutants (San et al., 2016, van der
359 Velden et al., 2012), but also in other animal models (Kennison, 1995). Other transcription factors,
360 such as the *tbx* gene family members, showed more diverse patterns of deregulation compared to
361 *hox* genes. ISH and RT-qPCR showed that, among the *tbx* genes examined, some were overexpressed
362 outside their normal expression domains (*tbx2a, tbx3a, and tbx5a*), whereas others were also
363 ubiquitously upregulated (*tbx3a* and *tbx5a*). The case of eye patterning is a good example of the
364 defect in control of gene expression pattern in *MZezh2* mutant embryos. In wildtype embryos, at 24
365 hpf, *tbx* genes are expressed in the dorsal part of the eye whereas *isl1* is expressed in the ventral
366 part. Upon loss of Ezh2, our ISH results showed that the expression of the *tbx* genes expands to the
367 whole eye whereas *isl1* disappears from the ventral region. We conclude that Polycomb-mediated
368 repression is therefore responsible for maintenance of expression domains rather than control of
369 expression level at this time of development in the zebrafish embryo.

370 Expression analysis by ISH for *tbx* and *hox* genes as well as for *isl1* also showed loss of expression in
371 specific structures in *MZezh2* mutant embryos. We reasoned that the absence of expression of *hox*
372 and *tbx* genes in the fin bud could be a secondary effect due to the absence of this structure in
373 *MZezh2* mutants (San et al., 2016). The same phenomenon could explain the lack of detection of
374 *tbx2b* and *isl1* in pharyngeal arches, pronephros, and lateral line ganglions. The case of *gsc*
375 expression is more striking, as its normal expression pattern is totally abolished and a ubiquitous
376 expression pattern is detected. The *gsc* gene is known to be expressed in the Spemann organizer
377 during gastrulation and therefore all cells will transiently express *gsc* when undergoing gastrulation
378 (Joubin and Stern, 1999, Stachel et al., 1993). In absence of Ezh2, *gsc* expression could remain active
379 in all cells after leaving the Spemann organizer, leading to a ubiquitous expression pattern and
380 impaired tissue specific expression in 24 hpf *MZezh2* mutant embryos.

381 To conclude, our results show that major characteristics of PcG-mediated repression are conserved
382 in zebrafish, including canonical recruitment or PcG complexes and their function in maintenance of
383 pre-established gene expression patterns. Our use of a mutant depleted of both maternal and
384 zygotic contribution of Ezh2 also reveals that no PRC2-independent recruitment of PRC1 occurs at
385 this stage of development. Finally, we demonstrate that early embryonic development, including
386 germ layer formation and cell fate specification, is independent of PcG-mediated gene repression
387 until axis are formed and organs specified. PcG-mediated gene repression is then required to control
388 precise spatial restricted expression of specific transcription factors. We hypothesize that subtle

389 changes in expression of these important genes subsequently will lead to progressive and
390 accumulating changes in gene network regulation and result in loss of tissue identity maintenance.

391 This surprising result highlights the fact that, despite the conservation of PcG-mediated repression
392 mechanisms during evolution, the time frame within which PcG repression is required for proper
393 development may vary greatly between species. Studying the PcG repression in additional species
394 would improve our understanding of the importance of PcG biology during development.

395

396

397 **Materials and methods**

398 **Zebrafish genetics and strains**

399 Zebrafish (*Danio rerio*), were housed according to standard conditions (Westerfield, 2000) and
400 staged according to Kimmel et al. (Kimmel et al., 1995). The *ezh2* nonsense mutant (*hu5670*) (San et
401 al., 2016), *Tg (H2A::GFP)* (Pauls et al., 2001), and *Tg (vas::eGFP)* (Krovel and Olsen, 2002) zebrafish
402 lines have been described before. Genotyping of the *ezh2* allele was performed as previously
403 described (San et al., 2016) with following adaptations: different primer pairs were used for PCR and
404 nested PCR (Table S2), of which the restriction profile is shown on Fig. S1F. All experiments were
405 carried out in accordance with animal welfare laws, guidelines, and policies and were approved by
406 the Radboud University Animal Experiments Committee.

407

408 **Germ cell transplantation**

409 Germ cell transplantation was performed as described previously (San et al., 2016). For all
410 experiments below, *ezh2* germline mutant females were crossed with *ezh2* germline mutant males
411 to obtain 100% *MZezh2* mutant progeny. The germline wild-type sibling males and females obtained
412 during transplantation were used to obtain 100% wildtype progeny with similar genetic background
413 and are referred to as wildtype. The embryos used were all from the first generation after germline
414 transplantation.

415

416 **Western blotting**

417 At 3.3 hpf, 50 embryos were collected, resuspended in in 500 µl ½ Ringer solution (55 mM NaCl, 1.8
418 mM KCl, 1.25 mM $NaHCO_3$) and forced through a 21G needle and a cell strainer in order to remove
419 the chorion and disrupt the yolk. At 24 hpf, 20 embryos were collected and resuspended by
420 thorough pipetting in 500µl ½ Ringer solution in order to disrupt the yolk. The samples of 3.3 and 24

421 hpf were centrifuged for 5 minutes at 3,500 g at 4°C and washed two additional times with 500 µl ½
422 Ringer solution. The embryo pellet was frozen in liquid nitrogen and stored at -80°C. Whole protein
423 extraction was performed by adding 40 µl of RIPA buffer (100 mM Tris-HCl pH 8, 300 mM NaCl, 2%
424 NP-40, 1% Sodium Deoxycholate, 0.2% SDS, 20% glycerol, 1x cOmplete EDTA-free protease inhibitor
425 cocktails from Sigma) and sonication for 2 cycles of 15s ON and 15s OFF on medium power at 4°C on
426 a PicoBioruptor (Diagenode). After 10 minutes incubation at 4°C, embryo lysates were centrifuged
427 for 12 minutes at 16,000 g at 4°C and supernatant was transferred in a new tube. 20 µg protein was
428 mixed with SDS containing sample loading buffer, denaturated at 95°C for 5 minutes and analyzed by
429 Western blot analysis. Antibodies used for immunoblotting are described in Table S3 HRP-
430 conjugated anti-rabbit secondary antibody was used (Table S3) and protein detection was
431 performed with ECL Select Western Blotting Detection Reagent (GE Healthcare, RPN2235) on an
432 ImageQuant LAS 4000 (GE Healthcare) Western-blot anti-H2A western-blot were performed on
433 histone extract according to van der Velden et al. (van der Velden et al., 2012), and detected on X-
434 ray film.
435
436 **ChIP-sequencing**
437 For chromatin preparation, embryos from a germline mutant or germline wildtype incross were
438 collected at 24 hpf and processed per batches of 300 embryos. Embryos were first dechorionated by
439 pronase (0.6 µg/µl) treatment and then extensively washed with E3 medium. Subsequently, embryos
440 were fixed in 1% PFA (EMS, 15710) for 15 minutes at room temperature and fixation was terminated
441 by adding 0.125M glycine and washed 3 times in cold PBS. Yolk from fixed embryos was disrupted by
442 pipetting the fixed embryos 10 times with a 1 ml tip in 600 µl of ½ Ringer solution (55 mM NaCl, 1.8
443 mM KCl, 1.25 mM $NaHCO_3$) and incubated for 5 minutes at 4°C on a rotating wheel. Embryos were
444 pelleted by centrifuging 30 seconds at 300 g and the supernatant was removed. De-yolked embryos
445 were resuspended in 600 µl sonication buffer (20 mM Tris-HCl pH 7.5, 70 mM KCl, 1 mM EDTA, 10%
446 glycerol, 0.125% NP40, 1x cOmplete EDTA-free protease inhibitor cocktails from Sigma) and
447 homogenized with a Dounce homogenizer (6 strokes with pestle A, followed by 6 strokes with pestle
448 B). Homogenates were sonicated for 6 cycles of 30 seconds ON/30 seconds OFF on a PicoBioruptor
449 (Diagenode), centrifuged for 10 minutes at 16,000 g at 4°C, and the supernatant containing the
450 chromatin was stored at -80°C. 20 µl of the supernatant was subjected to phenol-chloroform
451 extraction and ran on an agarose gel to verify that a proper chromatin size of 200-400 bp was
452 obtained.
453 For ChIP, 100 µl of chromatin preparation (corresponding to 50 embryos) was mixed with 100 µl IP-
454 buffer (50 mM Tris-HCL pH 7.5, 100 mM NaCl, 2 mM EDTA, 1% NP-40, 1x cOmplete EDTA-free

455 protease inhibitor cocktails from Sigma) and antibody (for details on antibodies used see Table S3)
456 and incubated overnight at 4°C on a rotating wheel. When relevant, *Drosophila* chromatin and anti-
457 H2Av were used according to manufacturer's instructions were followed (Active Motif, 53093 and
458 61686). For immunoprecipitation, 20 µl of protein G magnetic beads (Invitrogen, 1003D) were
459 washed in IP buffer and then incubated with the chromatin mix for 2 hours at 4°C on a rotating
460 wheel. Samples were washed in 500 µl washing buffer 1 (IP-buffer + 0.1% Sodium Deoxycholate),
461 followed by washing in washing buffer 2 (washing buffer 1 + 400mM NaCl), washing buffer 3
462 (washing buffer 1 + 250mM LiCl), washing buffer 1 and a final wash in 250 µl of TE buffer. All washes
463 were 5 minutes at 4°C on a rotating wheel. Chromatin was eluted from the beads by incubation in
464 100 µl of elution buffer (50 mM $NaHCO_3$ pH 8.8, 1% SDS) for 15 minutes at 65°C at 900 rpm in a
465 thermomixer. The supernatant was transferred in a clean 1.5 ml tube. Elution was repeated a second
466 time and both supernatants were pooled. The eluate was treated with 0.33 µg/µl RNaseA for 2 hours
467 at 37°C. Samples were then decrosslinked by adding 10 µl of 4M NaCL and 1 µl of 10mg/ml
468 proteinase K and incubated overnight at 65°C. DNA was then purified using MinElute Reaction Clean-
469 Up kit (Qiagen, 28204).
470 1-5 ng of DNA was used to prepare libraries with the KAPA Hyper Prep Kit (KAPABiosystems, KK8504)
471 and NEXTflex ChIP-Seq Barcodes for Illumina (Bioo Scientific, 514122) followed by paired-end 43bp
472 sequencing on an Illumina NextSeq500 platform. All ChIP-seq were performed in two biological
473 replicates, except for Rnf2 in wildtype embryos which was performed once and H3K27ac which was
474 performed in triplicate in both wildtype and mutant embryos.
475
476 **RNA-sequencing**
477 Ten to twenty manually dechorionated 24 hpf embryos of a germline mutant incross and a germline
478 wildtype incross were homogenized in TRIzol (Ambion, 15596018). Subsequently, the Quick RNA
479 microprep kit (Zymo Research, R1051) was used to isolate RNA and treat the samples with DNAseI.
480 Most samples were depleted from rRNA using the Ribo-Zero rRNA Removal Kit (Illumina,
481 MRZH11124), followed by fragmentation, cDNA synthesis, and libraries were generated using the
482 KAPA Hyper Prep Kit (KAPABiosystems, KK8504). Sequencing libraries were paired-end sequenced
483 (43 bp read-length) on an Illumina NextSeq500 platform. However, two samples per genotype were
484 generated with the TruSeq Stranded Total RNA Library Prep Kit with Ribo-Zero (Illumina, RS-122-
485 2201) and single-end sequenced (50 bp read-length) on an Illumina HiSeq 2500. For wildtype and
486 *MZezh2* mutant embryos, 6 and 7 biological replicates were used, respectively.
487
488 **Mass spectrometry**

489 At 24 hpf, 50 embryos were collected, dechorionated, and resuspended by gently pipetting in 500 µl
490 deyolking buffer (1/2 Ginzburg Fish Ringer without Calcium: 55 mM NaCl, 1.8 mM KCl, 1.25 mM
491 NaHCO3, 1x cOmplete EDTA-free protease inhibitor cocktail from Sigma) and incubated for 5
492 minutes in a Thermomixer at RT at 1,100 rpm to disrupt the yolk. The samples were then centrifuged
493 for 30 seconds at 400 g and the pellet was washed two times in 0.5 ml wash buffer (110 mM NaCl,
494 3.5 mM KCl, 2.7 mM CaCl2, 10mM Tris/Cl pH8.5, 1x cOmplete EDTA-free protease inhibitor cocktail
495 from Sigma) for 2 minutes in a Thermomixer at RT and 1,100 rpm, followed by 30 seconds
496 centrifugation at 400 g. Washed pellets were lysed in 100 µl RIPA buffer (50 mM Tris pH8.0, 150 mM
497 NaCl, 0.1% SDS, 1% NP-40, 0.5% DOC, 20% glycerol, 1 mM Sodium Orthovanadate, 1x cOmplete
498 EDTA-free protease inhibitor cocktails from Sigma) and sonicated for 2 cycles of 15s ON and 15s OFF
499 on full power at 4°C on a Bioruptor (Diagenode). Samples were incubated for 1 hour on a rotating
500 wheel at 4°C and centrifuged 10 minutes at 12,000 g and 4°C. Supernatant was flash frozen and
501 stored at -80°C. After Bradford analysis, 100 µg protein lysate was used for FASP-SAX as previously
502 described (Wisniewski et al., 2011). The peptide fractions were separated on an Easy nLC 1000
503 (Thermo Scientific) connected to a Thermo scientific Orbitrap Fusion Tribrid mass spectrometer. MS
504 and MS/MS spectra were recorded in a top speed modus with a run cycle of 3s using Higher- energy
505 Collision Dissociation (HCD) fragmentation. The raw mass spectrometry data were analyzed using
506 the MAXQuant software version 1.6.0.1 (http://www.ncbi.nlm.nih.gov/pubmed/19029910) with
507 default settings. Data was searched against the *Danio rerio* data base (UniProt June 2017). The
508 experiment was performed with biological triplicates for each condition.
509
510 **Bioinformatics analyses**
511 For ChIP-seq analysis, fastq files were aligned to GRCz10 zebrafish genome version using BWA-MEM
512 (version 0.7.10-r789) for paired-end reads (Li and Durbin, 2009). Duplicated and multimapping reads
513 were removed using samtools (Li et al., 2009) version 1.2 and Picard tools
514 (http://broadinstitute.github.io/picard) version 2.14.1. When spike-in normalization was used,
515 *Drosophila* reads were aligned to dm6 *Drosophila* genome version and a normalization factor was
516 then applied to zebrafish reads according to manufacturer's protocol (Active Motif, 53093 and
517 61686). MACS2 (Zhang et al., 2008) version 2.1.1 was used to call peaks from each aligned bam files
518 using an Input track from 24 hpf wild-type embryos as control sequence. Peaks separated by less
519 than 1kb distance were merged, peaks that were called using Input alone were removed from all
520 data sets using bedtools suit version 2.20.1, and the intersection between the replicates for each
521 antibody in each condition was used to define the definitive peak sets. For visualization in heatmaps
522 and genome browser snapshots, fastq files from duplicate ChIP-sequencing were merged, aligned as

523 described above, subsampled to equalized read numbers between wildtype and *MZezh2* mutant
524 conditions for each ChIP, and transformed into bigwig alignment files using bam2bw version 1.25.
525 Peak lists were analyzed using bedtools and heatmaps were produced using deepTools plotHeatmap
526 (Ramirez et al., 2016) version 2.5.3. Comparison between H3K4me3 peaks in *MZezh2* mutant and
527 wildtype conditions was performed using DiffBind version 2.10.0 on the union between H3K4me3
528 peaks detected in both conditions.
529 For RNA-sequencing analysis, read counts per gene were retrieve using GeneCounts quantification
530 method from STAR (Dobin et al., 2013) version 2.4.0 and the GRCz10 zebrafish genome version with
531 Ensembl annotation version 87 as reference. Differential expression analysis was calculated with
532 DESeq2 (Love et al., 2014) version 1.14.1.
533 For proteomics analysis, differential expression of protein between conditions was assessed with
534 DEP (Zhang et al., 2018) version 1.2.0.
535 Gene Ontology analyses on selected genes were performed using DAVID bioinformatics resources
536 (Huang da et al., 2009) version 6.8 and anatomical term enrichment was done using ZEOGS
537 (Prykhozhij et al., 2013).
538
539 **Whole mount *in situ* hybridization**
540 Embryos at 24 hpf were dechorionated and fixed overnight at 4°C in 4% PFA in PBST (0.1% Tween),
541 after which they were gradually transferred to 100% methanol. Prior to ISH, embryos were gradually
542 transferred back to PBST and, subsequently, ISH was performed as described previously (Houwing et
543 al., 2007). The embryos were imaged by light microscopy on a Leica MZFLIII, equipped with a DFC450
544 camera.
545
546 **RT-qPCR analyses**
547 Total RNA was isolated using Trizol from 20 flash-frozen dechorionated 24 hpf wildtype and *MZezh2*
548 mutant embryos cut in two with tweezers. Reverse transcription was achieved using Superscript III
549 (Invitrogen, 18080093) and poly-dT primers. Standard qPCR using SYBR Green (iQ SYBR Green
550 Supermix, BioRad, 1708880) was performed using the primers shown in Table S2. Relative
551 expression was calculated based on expression of housekeeping genes *β-actin*. Calculations were
552 based on at least 3 independent replicates for both conditions.
553
554
555 **Acknowledgements**

556 We thank J. Bakkers, from the Hubrecht Institute, for providing the *tbx2a*, *tbx2b*, *tbx3a*, *tbx5a*, and
557 *isl1* plasmids and J. den Hertog from the Hubrecht Institute for providing the *gsc* plasmid for ISH
558 probe generation. We thank T. Spanings and A. van der Horst from the Radboud University for
559 excellent zebrafish husbandry and E. Janssen-Megens from the Radboud University for excellent
560 technical support. We thank R. Lindeboom, from the Radboud University, for computational advice.
561 We thank Dr. G.J.C. Veenstra, from the Radboud University, and his team for fruitful discussions. We
562 thank Dr. R. Knight, from the King's College London, for his help with ISH analysis.
563
564
565 **Competing interests**
566 The authors declare no competing interests.
567
568
569 **Funding**
570 The work was funded by the Innovative Research scheme of the Netherlands Organisation for
571 Scientific research (www.nwo.nl, NWO-Vidi 864.12.009, NWO-Meervoud 836.13.003 L.M.K.), the
572 Radboud University Nijmegen Medical Centre tenure track fellowship (www.radboudumc.nl, L.M.K.),
573 the European Union's Horizon 2020 research and innovation programme under the Marie
574 Skłodowska-Curie Grant (Agreement No. 705939, K.A.), the Howard Hughes Medical Institute and
575 the Huntsman Cancer Institute core facilities (CA24014, B.R.C.), and the Eunice Kennedy Shriver
576 National Institute of Child Health and Human Development of the NIH (T32HD007491, P.J.M.).
577
578
579 **Data availability**
580 The sequencing data have been submitted to the NCBI Gene Expression Omnibus (GEO;
581 http://www.ncbi.nlm.nih.gov/geo/) under accession number GSE119070. The mass spectrometry
582 proteomics data have been deposited to the ProteomeXchange Consortium via the PRIDE (Vizcaino
583 et al., 2016) partner repository with the dataset identifier PXD010922. Reviewers can obtain access
584 to the datasets via login information provided to the editor.
585
586
587 **References**

588 BROCK, H. W. & FISHER, C. L. 2005. Maintenance of gene expression patterns. *Dev Dyn,* 232**,**
589 633-55.

590 CHITTOCK, E. C., LATWIEL, S., MILLER, T. C. & MULLER, C. W. 2017. Molecular architecture of
591 polycomb repressive complexes. *Biochem Soc Trans,* 45**,** 193-205.
592 CHRISPIJN, N. D., ANDRALOJC, K. M., CASTENMILLER, C. & KAMMINGA, L. M. 2018. Gene
593 expression profile of a selection of Polycomb Group genes during zebrafish embryonic and
594 germ line development. *PLoS One,* 13**,** e0200316.
595 CHRISPIJN, N. D., ELURBE, D. M., MICKOLEIT, M., ABEN, M., DE BAKKER, D. E. M.,
596 ANDRALOJC, K. M., HUISKEN, J., BAKKERS, J. & KAMMINGA, L. M. 2019. Loss of the Polycomb
597 group protein Rnf2 results in derepression of tbx-transcription factors and defects in
598 embryonic and cardiac development. *Sci Rep,* 9**,** 4327.
599 CIRUNA, B., WEIDINGER, G., KNAUT, H., THISSE, B., THISSE, C., RAZ, E. & SCHIER, A. F. 2002.
600 Production of maternal-zygotic mutant zebrafish by germ-line replacement. *Proc Natl Acad*
601 *Sci U S A,* 99**,** 14919-24.
602 CUNNINGHAM, T. J., ZHAO, X., SANDELL, L. L., EVANS, S. M., TRAINOR, P. A. & DUESTER, G.
603 2013. Antagonism between retinoic acid and fibroblast growth factor signaling during limb
604 development. *Cell Rep,* 3**,** 1503-11.
605 DOBIN, A., DAVIS, C. A., SCHLESINGER, F., DRENKOW, J., ZALESKI, C., JHA, S., BATUT, P.,
606 CHAISSON, M. & GINGERAS, T. R. 2013. STAR: ultrafast universal RNA-seq aligner.
607 *Bioinformatics,* 29**,** 15-21.
608 DUPRET, B., VOLKEL, P., VENNIN, C., TOILLON, R. A., LE BOURHIS, X. & ANGRAND, P. O. 2017.
609 The histone lysine methyltransferase Ezh2 is required for maintenance of the intestine
610 integrity and for caudal fin regeneration in zebrafish. *Biochim Biophys Acta,* 1860**,** 1079-
611 1093.
612 DYER, C., LINKER, C., GRAHAM, A. & KNIGHT, R. 2014. Specification of sensory neurons
613 occurs through diverse developmental programs functioning in the brain and spinal cord.
614 *Dev Dyn,* 243**,** 1429-39.
615 FAUST, C., LAWSON, K. A., SCHORK, N. J., THIEL, B. & MAGNUSON, T. 1998. The Polycomb-
616 group gene eed is required for normal morphogenetic movements during gastrulation in the
617 mouse embryo. *Development,* 125**,** 4495-506.
618 GAO, Z., ZHANG, J., BONASIO, R., STRINO, F., SAWAI, A., PARISI, F., KLUGER, Y. & REINBERG,
619 D. 2012. PCGF homologs, CBX proteins, and RYBP define functionally distinct PRC1 family
620 complexes. *Mol Cell,* 45**,** 344-56.
621 GRANDEL, H. & BRAND, M. 2011. Zebrafish limb development is triggered by a retinoic acid
622 signal during gastrulation. *Dev Dyn,* 240**,** 1116-26.

623 HE, J., SHEN, L., WAN, M., TARANOVA, O., WU, H. & ZHANG, Y. 2013. Kdm2b maintains
624 murine embryonic stem cell status by recruiting PRC1 complex to CpG islands of
625 developmental genes. *Nat Cell Biol,* 15**,** 373-84.
626 HEISENBERG, C. P., BRENNAN, C. & WILSON, S. W. 1999. Zebrafish aussicht mutant embryos
627 exhibit widespread overexpression of ace (fgf8) and coincident defects in CNS development.
628 *Development,* 126**,** 2129-40.
629 HOUWING, S., KAMMINGA, L. M., BEREZIKOV, E., CRONEMBOLD, D., GIRARD, A., VAN DEN
630 ELST, H., FILIPPOV, D. V., BLASER, H., RAZ, E., MOENS, C. B., PLASTERK, R. H., HANNON, G. J.,
631 DRAPER, B. W. & KETTING, R. F. 2007. A role for Piwi and piRNAs in germ cell maintenance
632 and transposon silencing in Zebrafish. *Cell,* 129**,** 69-82.
633 HUANG DA, W., SHERMAN, B. T. & LEMPICKI, R. A. 2009. Systematic and integrative analysis
634 of large gene lists using DAVID bioinformatics resources. *Nat Protoc,* 4**,** 44-57.
635 JOUBIN, K. & STERN, C. D. 1999. Molecular interactions continuously define the organizer
636 during the cell movements of gastrulation. *Cell,* 98**,** 559-71.
637 KENNISON, J. A. 1995. The Polycomb and trithorax group proteins of Drosophila: trans-
638 regulators of homeotic gene function. *Annu Rev Genet,* 29**,** 289-303.
639 KIMMEL, C. B., BALLARD, W. W., KIMMEL, S. R., ULLMANN, B. & SCHILLING, T. F. 1995. Stages
640 of embryonic development of the zebrafish. *Dev Dyn,* 203**,** 253-310.
641 KLOET, S. L., MAKOWSKI, M. M., BAYMAZ, H. I., VAN VOORTHUIJSEN, L., KAREMAKER, I. D.,
642 SANTANACH, A., JANSEN, P., DI CROCE, L. & VERMEULEN, M. 2016. The dynamic interactome
643 and genomic targets of Polycomb complexes during stem-cell differentiation. *Nat Struct Mol*
644 *Biol,* 23**,** 682-690.
645 KLYMENKO, T. & MULLER, J. 2004. The histone methyltransferases Trithorax and Ash1
646 prevent transcriptional silencing by Polycomb group proteins. *EMBO Rep,* 5**,** 373-7.
647 KROVEL, A. V. & OLSEN, L. C. 2002. Expression of a vas::EGFP transgene in primordial germ
648 cells of the zebrafish. *Mech Dev,* 116**,** 141-50.
649 LAURSEN, K. B., MONGAN, N. P., ZHUANG, Y., NG, M. M., BENOIT, Y. D. & GUDAS, L. J. 2013.
650 Polycomb recruitment attenuates retinoic acid-induced transcription of the bivalent NR2F1
651 gene. *Nucleic Acids Res,* 41**,** 6430-43.
652 LE FAOU, P., VOLKEL, P. & ANGRAND, P. O. 2011. The zebrafish genes encoding the
653 Polycomb repressive complex (PRC) 1. *Gene,* 475**,** 10-21.
654 LI, G. & REINBERG, D. 2011. Chromatin higher-order structures and gene regulation. *Curr*
655 *Opin Genet Dev,* 21**,** 175-86.

656 LI, H. & DURBIN, R. 2009. Fast and accurate short read alignment with Burrows-Wheeler
657 transform. *Bioinformatics,* 25**,** 1754-60.
658 LI, H., HANDSAKER, B., WYSOKER, A., FENNELL, T., RUAN, J., HOMER, N., MARTH, G.,
659 ABECASIS, G., DURBIN, R. & GENOME PROJECT DATA PROCESSING, S. 2009. The Sequence
660 Alignment/Map format and SAMtools. *Bioinformatics,* 25**,** 2078-9.
661 LINDEMAN, L. C., ANDERSEN, I. S., REINER, A. H., LI, N., AANES, H., OSTRUP, O., WINATA, C.,
662 MATHAVAN, S., MULLER, F., ALESTROM, P. & COLLAS, P. 2011. Prepatterning of
663 developmental gene expression by modified histones before zygotic genome activation. *Dev*
664 *Cell,* 21**,** 993-1004.
665 LOUBIERE, V., DELEST, A., THOMAS, A., BONEV, B., SCHUETTENGRUBER, B., SATI, S.,
666 MARTINEZ, A. M. & CAVALLI, G. 2016. Coordinate redeployment of PRC1 proteins suppresses
667 tumor formation during Drosophila development. *Nat Genet,* 48**,** 1436-1442.
668 LOVE, M. I., HUBER, W. & ANDERS, S. 2014. Moderated estimation of fold change and
669 dispersion for RNA-seq data with DESeq2. *Genome Biol,* 15**,** 550.
670 LUPO, G., LIU, Y., QIU, R., CHANDRARATNA, R. A., BARSACCHI, G., HE, R. Q. & HARRIS, W. A.
671 2005. Dorsoventral patterning of the Xenopus eye: a collaboration of Retinoid, Hedgehog
672 and FGF receptor signaling. *Development,* 132**,** 1737-48.
673 MALLO, M. & ALONSO, C. R. 2013. The regulation of Hox gene expression during animal
674 development. *Development,* 140**,** 3951-63.
675 MARGUERON, R., LI, G., SARMA, K., BLAIS, A., ZAVADIL, J., WOODCOCK, C. L., DYNLACHT, B.
676 D. & REINBERG, D. 2008. Ezh1 and Ezh2 maintain repressive chromatin through different
677 mechanisms. *Mol Cell,* 32**,** 503-18.
678 MARSH-ARMSTRONG, N., MCCAFFERY, P., GILBERT, W., DOWLING, J. E. & DRAGER, U. C.
679 1994. Retinoic acid is necessary for development of the ventral retina in zebrafish. *Proc Natl*
680 *Acad Sci U S A,* 91**,** 7286-90.
681 MAVES, L. & KIMMEL, C. B. 2005. Dynamic and sequential patterning of the zebrafish
682 posterior hindbrain by retinoic acid. *Dev Biol,* 285**,** 593-605.
683 MCGINNIS, W. & TICKLE, C. 2005. Pattern formation and developmental mechanisms: good
684 mileage from comparative studies in cell biology, gene regulation, development and
685 evolution. *Curr Opin Genet Dev,* 15**,** 355-7.
686 MIKKELSEN, T. S., KU, M., JAFFE, D. B., ISSAC, B., LIEBERMAN, E., GIANNOUKOS, G., ALVAREZ,
687 P., BROCKMAN, W., KIM, T. K., KOCHE, R. P., LEE, W., MENDENHALL, E., O'DONOVAN, A.,
688 PRESSER, A., RUSS, C., XIE, X., MEISSNER, A., WERNIG, M., JAENISCH, R., NUSBAUM, C.,

689 LANDER, E. S. & BERNSTEIN, B. E. 2007. Genome-wide maps of chromatin state in
690 pluripotent and lineage-committed cells. *Nature,* 448**,** 553-60.
691 MURPHY, P. J., WU, S. F., JAMES, C. R., WIKE, C. L. & CAIRNS, B. R. 2018. Placeholder
692 Nucleosomes Underlie Germline-to-Embryo DNA Methylation Reprogramming. *Cell,* 172**,**
693 993-1006 e13.
694 O'CARROLL, D., ERHARDT, S., PAGANI, M., BARTON, S. C., SURANI, M. A. & JENUWEIN, T.
695 2001. The polycomb-group gene Ezh2 is required for early mouse development. *Mol Cell*
696 *Biol,* 21**,** 4330-6.
697 PASINI, D., BRACKEN, A. P., JENSEN, M. R., LAZZERINI DENCHI, E. & HELIN, K. 2004. Suz12 is
698 essential for mouse development and for EZH2 histone methyltransferase activity. *EMBO J,*
699 23**,** 4061-71.
700 PAULS, S., GELDMACHER-VOSS, B. & CAMPOS-ORTEGA, J. A. 2001. A zebrafish histone
701 variant H2A.F/Z and a transgenic H2A.F/Z:GFP fusion protein for in vivo studies of embryonic
702 development. *Dev Genes Evol,* 211**,** 603-10.
703 PIUNTI, A. & SHILATIFARD, A. 2016. Epigenetic balance of gene expression by Polycomb and
704 COMPASS families. *Science,* 352**,** aad9780.
705 POTOK, M. E., NIX, D. A., PARNELL, T. J. & CAIRNS, B. R. 2013. Reprogramming the maternal
706 zebrafish genome after fertilization to match the paternal methylation pattern. *Cell,* 153**,**
707 759-72.
708 PRINCE, V. E., JOLY, L., EKKER, M. & HO, R. K. 1998. Zebrafish hox genes: genomic
709 organization and modified colinear expression patterns in the trunk. *Development,* 125**,** 407-
710 20.
711 PRYKHOZHIJ, S. V., MARSICO, A. & MEIJSING, S. H. 2013. Zebrafish Expression Ontology of
712 Gene Sets (ZEOGS): a tool to analyze enrichment of zebrafish anatomical terms in large gene
713 sets. *Zebrafish,* 10**,** 303-15.
714 RAMIREZ, F., RYAN, D. P., GRUNING, B., BHARDWAJ, V., KILPERT, F., RICHTER, A. S., HEYNE,
715 S., DUNDAR, F. & MANKE, T. 2016. deepTools2: a next generation web server for deep-
716 sequencing data analysis. *Nucleic Acids Res,* 44**,** W160-5.
717 RIBEIRO, I., KAWAKAMI, Y., BUSCHER, D., RAYA, A., RODRIGUEZ-LEON, J., MORITA, M.,
718 RODRIGUEZ ESTEBAN, C. & IZPISUA BELMONTE, J. C. 2007. Tbx2 and Tbx3 regulate the
719 dynamics of cell proliferation during heart remodeling. *PLoS One,* 2**,** e398.
720 SAMARUT, E., FRAHER, D., LAUDET, V. & GIBERT, Y. 2015. ZebRA: An overview of retinoic
721 acid signaling during zebrafish development. *Biochim Biophys Acta,* 1849**,** 73-83.

722 SAN, B., ABEN, M., ELURBE, D. M., VOELTZKE, K., DEN BROEDER, M. J., ROUGEOT, J., LEGLER,
723 J. & KAMMINGA, L. M. 2018. Genetic and Epigenetic Regulation of Zebrafish Intestinal
724 Development. *Epigenomes,* 2**,** 19.
725 SAN, B., CHRISPIJN, N. D., WITTKOPP, N., VAN HEERINGEN, S. J., LAGENDIJK, A. K., ABEN, M.,
726 BAKKERS, J., KETTING, R. F. & KAMMINGA, L. M. 2016. Normal formation of a vertebrate
727 body plan and loss of tissue maintenance in the absence of ezh2. *Sci Rep,* 6**,** 24658.
728 SANTOS-ROSA, H., SCHNEIDER, R., BANNISTER, A. J., SHERRIFF, J., BERNSTEIN, B. E., EMRE, N.
729 C., SCHREIBER, S. L., MELLOR, J. & KOUZARIDES, T. 2002. Active genes are tri-methylated at
730 K4 of histone H3. *Nature,* 419**,** 407-11.
731 SCHMITGES, F. W., PRUSTY, A. B., FATY, M., STUTZER, A., LINGARAJU, G. M., AIWAZIAN, J.,
732 SACK, R., HESS, D., LI, L., ZHOU, S., BUNKER, R. D., WIRTH, U., BOUWMEESTER, T., BAUER, A.,
733 LY-HARTIG, N., ZHAO, K., CHAN, H., GU, J., GUT, H., FISCHLE, W., MULLER, J. & THOMA, N. H.
734 2011. Histone methylation by PRC2 is inhibited by active chromatin marks. *Mol Cell,* 42**,** 330-
735 41.
736 SCHUETTENGRUBER, B., BOURBON, H. M., DI CROCE, L. & CAVALLI, G. 2017. Genome
737 Regulation by Polycomb and Trithorax: 70 Years and Counting. *Cell,* 171**,** 34-57.
738 SHEN, X., LIU, Y., HSU, Y. J., FUJIWARA, Y., KIM, J., MAO, X., YUAN, G. C. & ORKIN, S. H. 2008.
739 EZH1 mediates methylation on histone H3 lysine 27 and complements EZH2 in maintaining
740 stem cell identity and executing pluripotency. *Mol Cell,* 32**,** 491-502.
741 STACHEL, S. E., GRUNWALD, D. J. & MYERS, P. Z. 1993. Lithium perturbation and goosecoid
742 expression identify a dorsal specification pathway in the pregastrula zebrafish. *Development,*
743 117**,** 1261-74.
744 SUN, X. J., XU, P. F., ZHOU, T., HU, M., FU, C. T., ZHANG, Y., JIN, Y., CHEN, Y., CHEN, S. J.,
745 HUANG, Q. H., LIU, T. X. & CHEN, Z. 2008. Genome-wide survey and developmental
746 expression mapping of zebrafish SET domain-containing genes. *PLoS One,* 3**,** e1499.
747 TAMURA, K., YONEI-TAMURA, S. & IZPISUA BELMONTE, J. C. 1999. Differential expression of
748 Tbx4 and Tbx5 in Zebrafish fin buds. *Mech Dev,* 87**,** 181-4.
749 TAVARES, L., DIMITROVA, E., OXLEY, D., WEBSTER, J., POOT, R., DEMMERS, J., BEZSTAROSTI,
750 K., TAYLOR, S., URA, H., KOIDE, H., WUTZ, A., VIDAL, M., ELDERKIN, S. & BROCKDORFF, N.
751 2012. RYBP-PRC1 complexes mediate H2A ubiquitylation at polycomb target sites
752 independently of PRC2 and H3K27me3. *Cell,* 148**,** 664-78.
753 THISSE, B. T., C. 2004. Fast Release Clones: A High Throughput Expression Analysis. *ZFIN*
754 *Direct Data Submission (http://zfin.org).*

755 VAN DER VELDEN, Y. U., WANG, L., VAN LOHUIZEN, M. & HARAMIS, A. P. 2012. The
756 Polycomb group protein Ring1b is essential for pectoral fin development. *Development,* 139**,**
757 2210-20.
758 VASTENHOUW, N. L., ZHANG, Y., WOODS, I. G., IMAM, F., REGEV, A., LIU, X. S., RINN, J. &
759 SCHIER, A. F. 2010. Chromatin signature of embryonic pluripotency is established during
760 genome activation. *Nature,* 464**,** 922-6.
761 VIZCAINO, J. A., CSORDAS, A., DEL-TORO, N., DIANES, J. A., GRISS, J., LAVIDAS, I., MAYER, G.,
762 PEREZ-RIVEROL, Y., REISINGER, F., TERNENT, T., XU, Q. W., WANG, R. & HERMJAKOB, H.
763 2016. 2016 update of the PRIDE database and its related tools. *Nucleic Acids Res,* 44**,** D447-
764 56.
765 VONCKEN, J. W., ROELEN, B. A., ROEFS, M., DE VRIES, S., VERHOEVEN, E., MARINO, S.,
766 DESCHAMPS, J. & VAN LOHUIZEN, M. 2003. Rnf2 (Ring1b) deficiency causes gastrulation
767 arrest and cell cycle inhibition. *Proc Natl Acad Sci U S A,* 100**,** 2468-73.
768 WESTERFIELD, M. 2000. The zebrafish book. A guide for the laboratory use of zebrafish
769 (Danio rerio). 4th ed., Univ. of Oregon Press, Eugene.
770 WHITE, R. J., COLLINS, J. E., SEALY, I. M., WALI, N., DOOLEY, C. M., DIGBY, Z., STEMPLE, D. L.,
771 MURPHY, D. N., BILLIS, K., HOURLIER, T., FULLGRABE, A., DAVIS, M. P., ENRIGHT, A. J. &
772 BUSCH-NENTWICH, E. M. 2017. A high-resolution mRNA expression time course of
773 embryonic development in zebrafish. *Elife,* 6.
774 WHITE, R. J., NIE, Q., LANDER, A. D. & SCHILLING, T. F. 2007. Complex regulation of cyp26a1
775 creates a robust retinoic acid gradient in the zebrafish embryo. *PLoS Biol,* 5**,** e304.
776 WISNIEWSKI, J. R., OSTASIEWICZ, P. & MANN, M. 2011. High recovery FASP applied to the
777 proteomic analysis of microdissected formalin fixed paraffin embedded cancer tissues
778 retrieves known colon cancer markers. *J Proteome Res,* 10**,** 3040-9.
779 ZHANG, R., KNAPP, M., SUZUKI, K., KAJIOKA, D., SCHMIDT, J. M., WINKLER, J., YILMAZ, O.,
780 PLESCHKA, M., CAO, J., KOCKUM, C. C., BARKER, G., HOLMDAHL, G., BEAMAN, G., KEENE, D.,
781 WOOLF, A. S., CERVELLIONE, R. M., CHENG, W., WILKINS, S., GEARHART, J. P., SIRCHIA, F., DI
782 GRAZIA, M., EBERT, A. K., ROSCH, W., ELLINGER, J., JENETZKY, E., ZWINK, N., FEITZ, W. F.,
783 MARCELIS, C., SCHUMACHER, J., MARTINON-TORRES, F., HIBBERD, M. L., KHOR, C. C.,
784 HEILMANN-HEIMBACH, S., BARTH, S., BOYADJIEV, S. A., BRUSCO, A., LUDWIG, M., NEWMAN,
785 W., NORDENSKJOLD, A., YAMADA, G., ODERMATT, B. & REUTTER, H. 2017. ISL1 is a major
786 susceptibility gene for classic bladder exstrophy and a regulator of urinary tract
787 development. *Sci Rep,* 7**,** 42170.

788 ZHANG, X., SMITS, A. H., VAN TILBURG, G. B., OVAA, H., HUBER, W. & VERMEULEN, M. 2018.
789 Proteome-wide identification of ubiquitin interactions using UbIA-MS. *Nat Protoc,* 13**,** 530-
790 550.
791 ZHANG, Y., LIANG, J. & LI, Q. 2014. Coordinated regulation of retinoic acid signaling pathway
792 by KDM5B and polycomb repressive complex 2. *J Cell Biochem,* 115**,** 1528-38.
793 ZHANG, Y., LIU, T., MEYER, C. A., EECKHOUTE, J., JOHNSON, D. S., BERNSTEIN, B. E.,
794 NUSBAUM, C., MYERS, R. M., BROWN, M., LI, W. & LIU, X. S. 2008. Model-based analysis of
795 ChIP-Seq (MACS). *Genome Biol,* 9**,** R137.
796 ZHONG, Y., YE, Q., CHEN, C., WANG, M. & WANG, H. 2018. Ezh2 promotes clock function and
797 hematopoiesis independent of histone methyltransferase activity in zebrafish. *Nucleic Acids*
798 *Res,* 46**,** 3382-3399.
799 ZHU, P. & LI, G. 2016. Structural insights of nucleosome and the 30-nm chromatin fiber. *Curr*
800 *Opin Struct Biol,* 36**,** 106-15.

801

802

803 **Figures legends**

804

805 **Figure 1. *MZezh2* mutant (*MZezh2*$^{-/-}$) embryos lack Ezh2, H3K27me3, and Rnf2 binding to the**
806 **chromatin.** (**A**) *MZezh2*$^{+/-}$ (developing as wildtype embryos) and *MZezh2*$^{-/-}$ embryos at 24 and 48 hpf.
807 At 24 hpf, *MZezh2*$^{-/-}$ embryos lack a clear mid-hindbrain boundary compared to heterozygous
808 embryos (arrow head). At 48 hpf, *MZezh2*$^{-/-}$ embryos showed pleiotropic phenotypes compared to
809 heterozygous embryos, such as small eyes, small brain, heart edema, and blood accumulation in the
810 blood island (arrow heads). (**B**) Western blot analysis of Ezh2 at 3.3 hpf and 24 hpf of wildtype and
811 *MZezh2*$^{-/-}$ embryos. Histone H3 was used as a loading control. (**C**) Number of peaks called after Ezh2,
812 H3K27me3, and Rnf2 ChIP-seq of wildtype and *MZezh2*$^{-/-}$ embryos at 24hpf. Each peak set was
813 obtained by the intersection of two independent biological replicates. (**D**) Box plots of Ezh2,
814 H3K27me3, and Rnf2 RPKM-normalized coverage after respective ChIP-seq in wildtype and in
815 *MZezh2*$^{-/-}$ embryos at 24 hpf. The input control shown was obtained from wildtype embryos at 24
816 hpf. Coverages were calculated based on positions of peaks detected in wildtype embryos. t-test:
817 *** *P*-value < 0.001. (**E**) Heatmaps for Ezh2, H3K27me3, and Rnf2 subsampled counts after ChIP-seq
818 in 24 hpf wildtype and *MZezh2*$^{-/-}$ embryos. Windows of 10 kb regions for all H3K27me3 o Ezh2 peaks
819 in 24 hpf wildtype embryos are shown. The input track obtained from 24 hpf wildtype embryos was
820 used as control and was not subsampled. (**F, G**) UCSC genome browser snapshot depicting the loss of
821 Ezh2, H3K27me3, and Rnf2 after ChIP-seq in 24 hpf *MZezh2*$^{-/-}$ embryos compared to wildtype

822 embryos for (**F**) the *hoxab* gene cluster and (**G**) *tbx5a*. Colors represent ChIP-seq for different
823 proteins with blue: Ezh2, red: H3K27me3, purple: Rnf2, and grey: Input control.

824

825 **Figure 2. *MZezh2* mutant (*MZezh2*$^{-/-}$) embryos show an increase in H3K4me3 preferentially on**
826 **H3K27me3 targets.** (**A**) Number of peaks called after H3K4me3 ChIP-seq in wildtype and *MZezh2*$^{-/-}$
827 embryos at 24 hpf. Turquoise and green represent peaks shared by the two conditions and peaks
828 specific for one condition, respectively. (**B**) MA-plot showing the fold change ($\log_2$-transformed) in
829 H3K4me3 peak coverages in 24 hpf *MZezh2* mutant (*MZezh2*$^{-/-}$) and wildtype embryos as a function
830 of the normalized average count between the two conditions ($\log_{10}$-transformed) as calculated with
831 DiffBind on the union of H3K4me3 peaks detected in both wildtype and *MZezh2* mutant conditions.
832 Red: $\log_2$FC ≥ 1 or ≤-1 and *P*-adj < 0.05. (**C**) Heatmaps of subsampled counts after ChIP-seq for Ezh2
833 and H3K27me3 in wildtype embryos and H3K4me3 in wildtype and *MZezh2*$^{-/-}$ embryos at 24 hpf.
834 Heatmaps display peaks enriched or decreased in *MZezh2*$^{-/-}$ embryos compared with wildtypes. The
835 input track obtained from 24 hpf wildtype embryos was used as control. Blue, red, turquoise, and
836 grey represent ChIP-seq for Ezh2, H3K27me3, H3K4me3, and Input control, respectively. (**D**) Venn
837 diagrams presenting the overlap between peaks with increased or decreased H3K4me3 levels (gain
838 or loss) as detected by DiffBind with the presence of Ezh2 or H3K27me3 peaks within a +/-1 kb
839 window. Black numbers represent comparison between actual DiffBind results and ChIP-seq peaks
840 whereas grey numbers represent comparisons between actual DiffBind results and randomly
841 shuffled positions used as controls. X^2: *** *P*-value < 0.001, ** *P*-value < 0.01, * *P*-value < 0.05. (**E**)
842 UCSC browser snapshots of three genomic loci in wildtype and *MZezh2*$^{-/-}$ embryos at 24 hpf. Blue,
843 red, turquoise, and grey represent ChIP-seq for Ezh2, H3K27me3, H3K4me3, and Input control,
844 respectively. (**F**) Gene Ontology analysis of the closest genes restricted two 2kb upstream or
845 downstream from H3K4me3 peaks enriched in *MZezh2*$^{-/-}$.

846

847 **Figure 3. Loss of maternal zygotic *ezh2* results in overexpression of specific developmental genes.**
848 (**A**) MA-plot showing the fold change ($\log_2$-transformed) between gene expression in 24 hpf *MZezh2*
849 mutant (*MZezh2*$^{-/-}$) and wildtype embryos as a function of the normalized average count between
850 the two conditions ($\log_{10}$-transformed) as calculated with DEseq2. Turquoise: $\log_2$FC ≥ 1 and *P*-adj <
851 0.05, red: $\log_2$FC ≤ -1 and *P*-adj < 0.05. (**B**) Volcano plot showing the *P*-value (-$\log_{10}$-transformed) as a
852 function of the fold-change ($\log_2$-transformed) between protein expression level in *MZezh2* mutant
853 (*MZezh2*$^{-/-}$) compared to wildtype embryos at 24 hpf. (**C**) Gene Ontology of biological processes
854 analysis of genes upregulated (up) or downregulated (down) in *MZezh2*$^{-/-}$ embryos compared to

855 wildtype embryos at 24 hpf. (**D**) Analysis of anatomical terms associated with genes upregulated and
856 downregulated in *MZezh2*$^{-/-}$ embryos compared to wildtype embryos at 24 hpf. (**E**) Venn diagrams
857 presenting the overlap between genes upregulated (up) or downregulated (dn) in *MZezh2*$^{-/-}$ embryos
858 compared to wildtype and presence of H3K27me3 or H3K4me3 peaks. The closest genes from
859 H3K27me3 peaks in wildtype condition or H3K4me3 enriched (H3K4me3 up) and decreased
860 (H3K4me3 dn) peaks according to DiffBind were used for this analysis. Black numbers represent
861 comparison between actual DEseq2 identified genes and closest genes from peaks. Grey numbers
862 represent comparisons between actual DEseq2 identified genes and random selected genes used as
863 control. X^2: *** *P*-value < 0.001, ** *P*-value < 0.01, * *P*-value < 0.05. (**F**) Venn diagrams presenting the
864 overlap between proteins overrepresented (Protein up) or underrepresented (Protein dn) in
865 *MZezh2*$^{-/-}$ embryos compared to ChIP-seq and RNA-seq results. The closest genes from H3K27me3
866 peaks in wildtype condition or H3K4me3 enriched peaks according to DiffBind (H3K4me3 up) were
867 used for this analysis. Black numbers represent comparison between actual deregulated proteins
868 and genes. Grey numbers represent comparisons between actual deregulated proteins and random
869 selected genes used as control. X^2-test did not provide any significant results.

870

871 **Figure 4. Loss of maternal and zygotic *ezh2* results in ectopic expression of *hox* genes.** (**a**, **b**, **c**, **d**)
872 Expression analysis of (**A**) *hoxa9a,* (**B**) *hoxa9b*, (**C**) *hoxa11b,* and (**D**) *hoxa13b* at 24 hpf. Bar plots on
873 the left side of each panel represent relative expression of indicated *hox* genes in the anterior half
874 (red) and posterior half (turquoise) of wildtype and *MZezh2* mutant (*MZezh2*$^{-/-}$) embryos. Boxplots
875 on the right side of each panel represent normalized counts from RNA-seq experiments in *MZezh2*$^{-/-}$
876 and wildtype whole embryo lysates at 24 hpf. Above is a schematic representation of 1 dpf embryos.
877 Black boxes represent the expression domains of the *hox* genes in wildtype embryos based on
878 published data (Thisse, 2004). Dashed lines represent the demarcation between anterior (red) and
879 posterior (turquoise) parts of the embryo used for RT-qPCR analysis. For RT-qPCR, relative
880 expression was calculated based on expression of housekeeping gene *actb1*. Error bars represent
881 standard deviations. Relative expression was compared between anterior or posterior parts in
882 *MZezh2*$^{-/-}$ and wildtype embryos (one-way ANOVA with post-tests, *** *P*-value < 0.001, ** *P*-value <
883 0.01, * *P*-value < 0.05). For RNA-seq, adjusted *P*-values were extracted from Differential Expression
884 analysis with DEseq2.

885

886 **Figure 5. Transcription factor expression is spatially deregulated in *MZezh2* mutant (*MZezh2*$^{-/-}$)**
887 **embryos.** (**A**, **B**, **C**) Spatial expression analysis by (**A**) *in situ* hybridization (ISH), (**B**) RT-qPCR on

888 anterior half and posterior half, and (**C**) RNA-seq results of transcription factors *tbx2a, tbx2b, tbx3a*,
889 *tbx5a*, *isl1*, and *gsc* in 24 hpf embryos. In ISH, scale bars represent 1 mm. For RT-qPCR, relative
890 expression was calculated based on expression of housekeeping gene *actb1*. Error bars represent
891 standard deviations. Relative expression was compared between anterior (red) or posterior
892 (turquoise) parts in *MZezh2*$^{-/-}$ and wildtype embryos (one-way ANOVA with post-tests, *** *P*-value <
893 0.001, ** *P*-value < 0.01, * *P*-value < 0.05). Right boxplots represent normalized counts from RNA-
894 seq experiments in whole *MZezh2*$^{-/-}$ and wildtype embryos and adjusted *P*-values were taken from
895 Differential Expression analysis with DEseq2. all: anterior lateral lane ganglion, ba: branchial arch,
896 cmn: cranial motor neurons, de: diencephalon, drp: distal region of the pronephros, dscn: dorsal
897 spinal cord neurons, e: eye, ep: epiphysis, fn: forebrain nuclei, h: heart, hmn: hindbrain motor
898 neurons, llg: lateral lane ganglion, mot: primary motor neurons, og: olfactory ganglion, ov: otic
899 vesicle, pa: pharyngeal arches, pan: pancreas, pf: pectoral fin, pro: pronephros, sc: spinal cord, tdn:
900 telencephalon and diencephalon nuclei, te: telencephalon, vg: ventral ganglion.

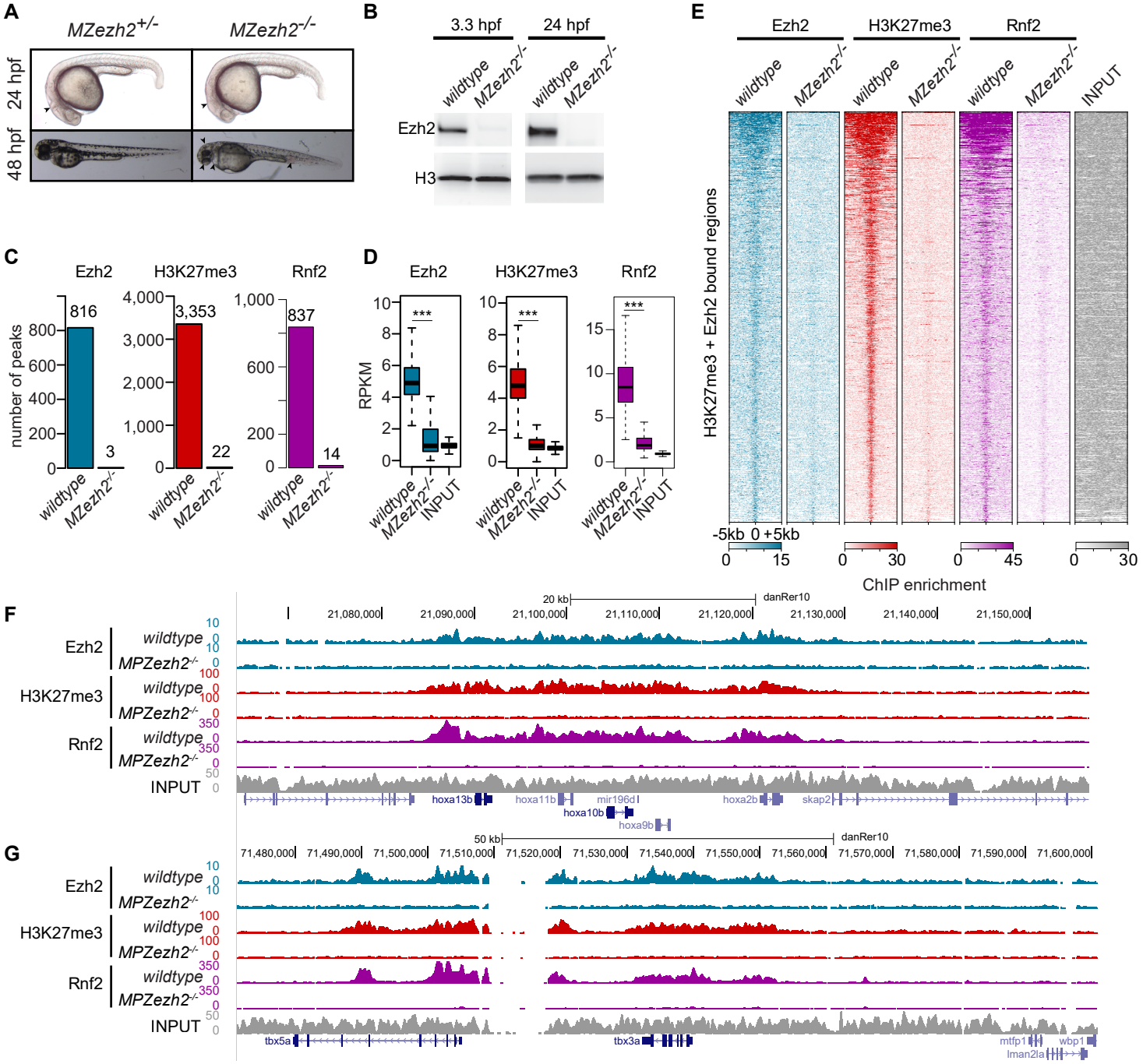

Rougeot_Fig. 1

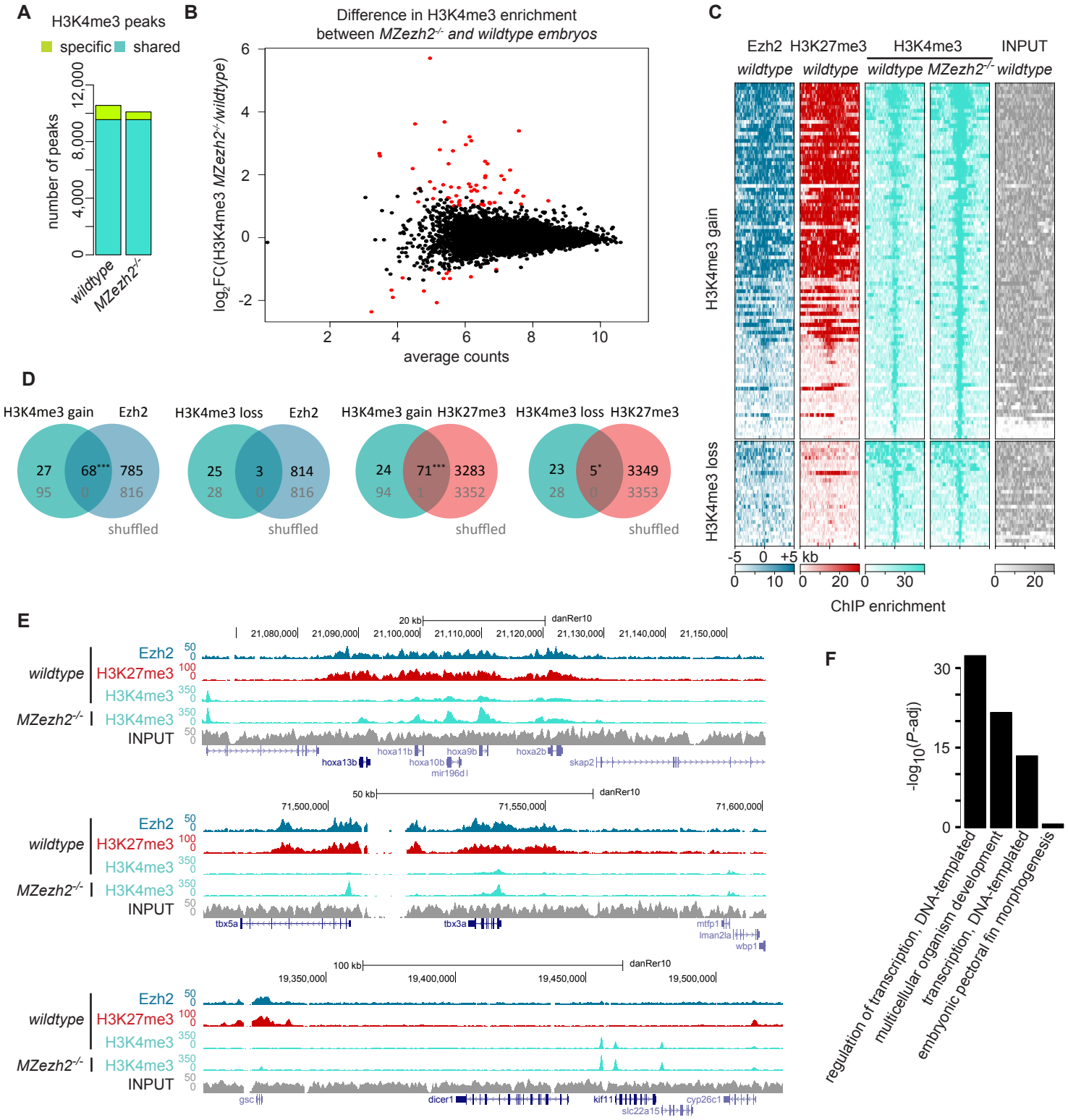

Rougeot_Fig. 2

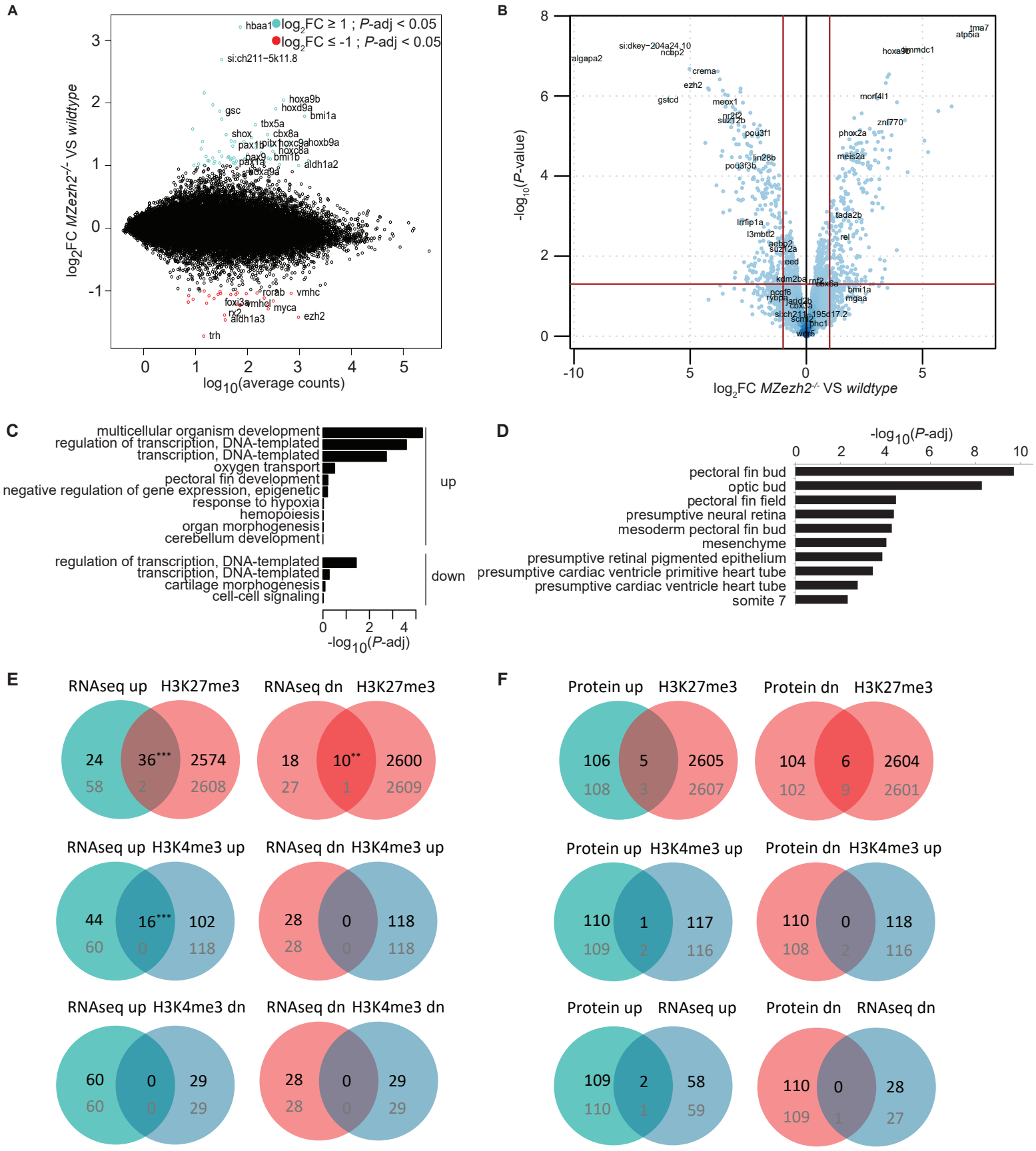

Rougeot_Fig. 3

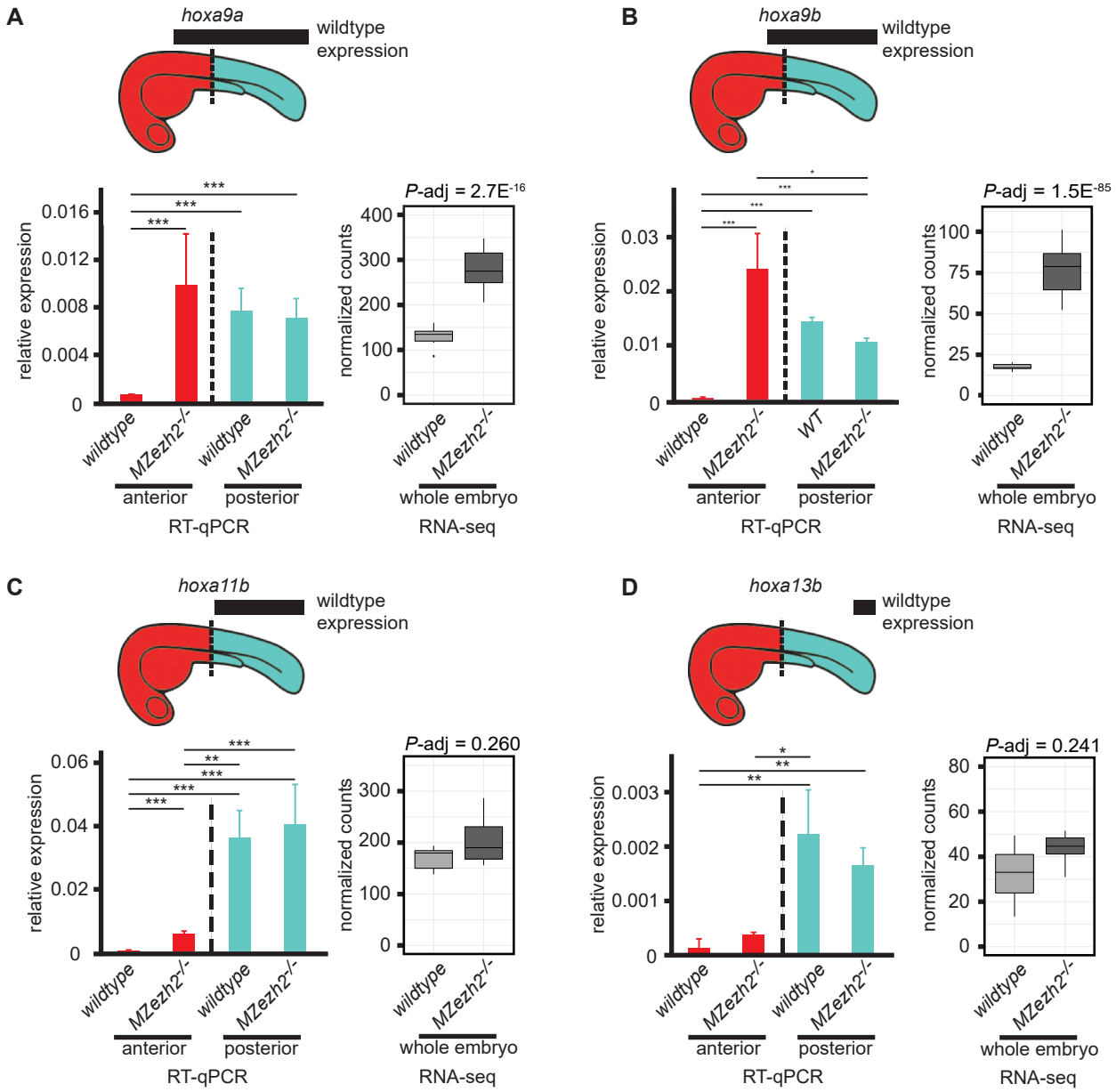

Rougeot_Fig. 4

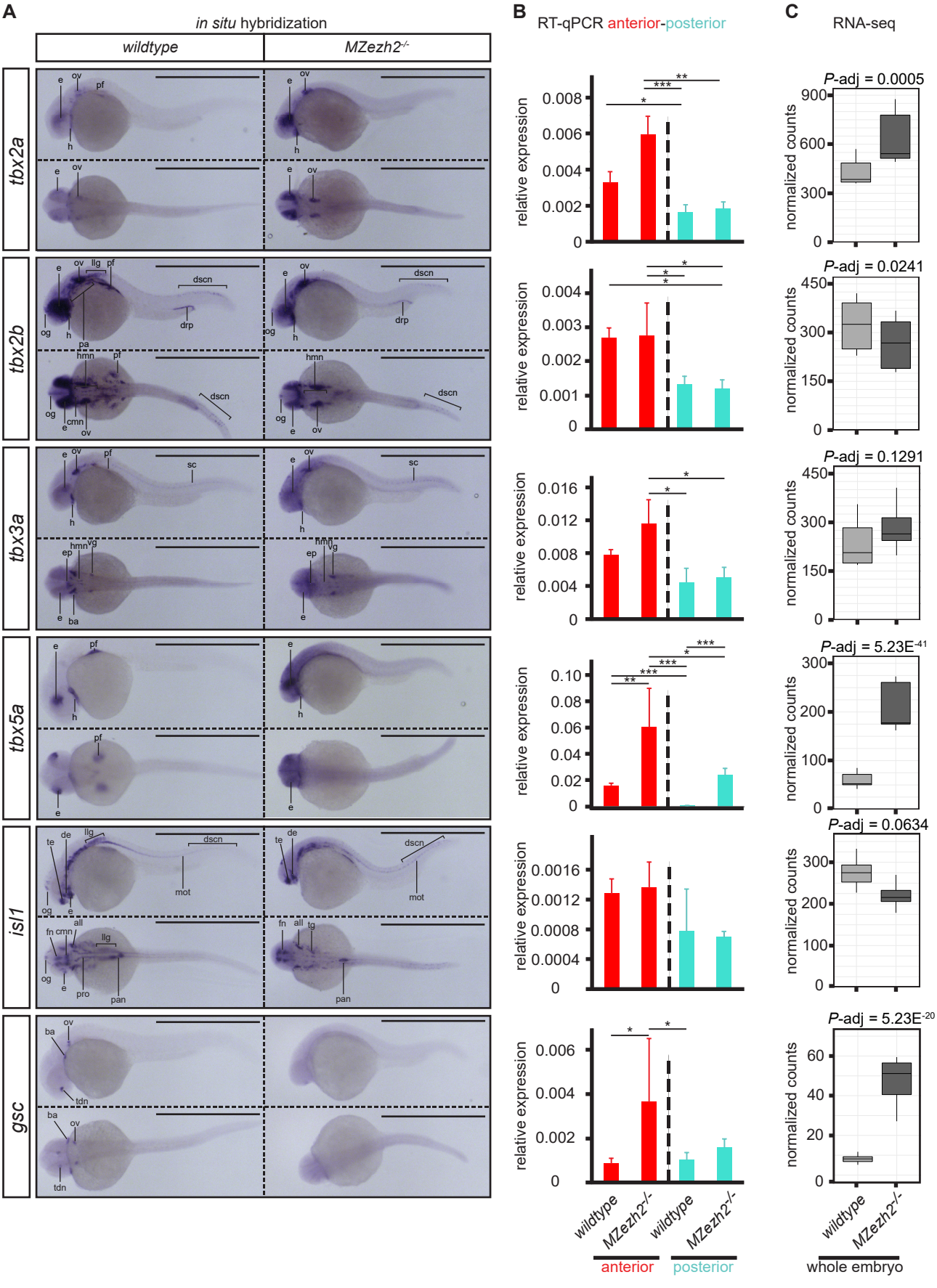

Rougeot_Fig. 5